Inorganic Chemistry

Article

pubs.acs.org/IC

Spin Delocalization Over Type Zero Copper

Alexey Potapov,[†,⊥] Kyle M. Lancaster,[‡,§] John H. Richards,[‡] Harry B. Gray,[‡] and Daniella Goldfarb*[,†]

[†]Department of Chemical Physics, Weizmann Institute of Science, Rehovot 76100, Israel

[‡]Beckman Institute, California Institute of Technology, Pasadena, California 91125, United States

Supporting Information

ABSTRACT: Hard-ligand, high-potential copper sites have been characterized in double mutants of *Pseudomonas aeruginosa* azurin (C112D/M121X (X = L, F, I)). These sites feature a small A_{zz}(Cu) splitting in the EPR spectrum together with enhanced electron transfer activity. Due to these unique properties, these constructs have been called "type zero" copper sites. In contrast, the single mutant, C112D, features a large A_{zz}(Cu) value characteristic of the typical type 2 Cu^{II}. In general, A_{zz}(Cu) comprises contributions from Fermi contact, spin dipolar, and orbital dipolar terms. In order to understand the origin of the low A_{zz}(Cu) value of type zero Cu^{II}, we explored in detail its degree of covalency, as manifested by spin delocalization over its ligands, which affects A_{zz}(Cu) through the Fermi contact and spin dipolar contributions. This was achieved by the application of several complementary EPR hyperfine spectroscopic techniques at X- and W-band (~9.5 and 95 GHz, respectively) frequencies to map the ligand hyperfine couplings. Our results show that spin delocalization over the ligands in type zero Cu^{II} is different from that of type 2 Cu^{II} in the single C112D mutant. The ^{14}N hyperfine couplings of the coordinated histidine nitrogens are smaller by about 25−40%, whereas that of the ^{13}C carboxylate of D112 is about 50% larger. From this comparison, we concluded that the spin delocalization of type zero copper over its ligands is not dramatically larger than in type 2 C112D. Therefore, the reduced A_{zz}(Cu) value of type zero Cu^{II} is largely attributable to an increased orbital dipolar contribution that is related to its larger g_{zz} value, as a consequence of the distorted tetrahedral geometry. The increased spin delocalization over the D112 carboxylate in type zero mutants compared to type 2 C112D suggests that electron transfer paths involving this residue are enhanced.

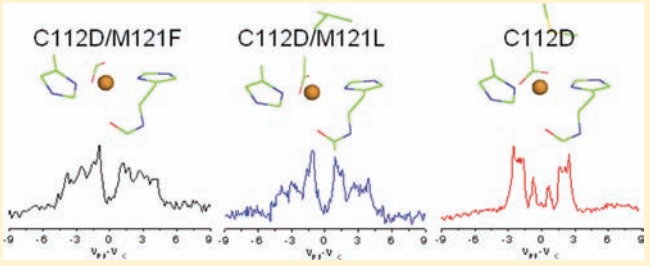

INTRODUCTION

All members of the blue copper protein family contain the unique type 1 copper site, which is involved in electron transfer (ET) reactions.[1] Blue copper proteins either function as discrete electron carriers (cupredoxins) or are incorporated as electron transfer domains in larger multisite proteins (e.g., multicopper oxidases).[2−5] The type 1 copper site has been subjected to thorough structural, spectroscopic, and kinetic studies.[6−13] The redox function of type 1 copper is achieved through a well-defined coordination environment consisting of two histidine nitrogens and a cysteine thiolate ligand (Figure 1a). In addition, there are relatively weak axial interactions by ancillary ligands such as a methionine thioether or a glutamine amide on one side (top) or a glycine backbone carbonyl on the other side (bottom), with coordination geometries ranging from trigonal-bipyramidal to pseudotetrahedral.[7,14,15] An outer-sphere hydrogen bonding network between backbone amides and the cysteine sulfur is largely responsible for the low ET reorganization energies that are signatures of these proteins.[14,15]

Type 1 copper exhibits an intense ($\varepsilon \sim 5000$ M^{-1} cm^{-1}) absorption band near 16 000 cm^{-1} attributable to a ligand to metal charge transfer (LMCT) transition that is responsible for its famous blue color.[9,16] The orbitals involved in the transition are π-bonding and π-antibonding combinations of sulfur 3p and Cu $3d_{x^2-y^2}$, not their corresponding σ components. The π-antibonding combination is singly occupied in the electronic ground state, and π-covalency is extensive,[17,18] owing to overlap between energetically well-matched thiolate and copper d orbitals. This results in an exceptionally strong electronic coupling between the protein and the metal center[19] as well as the remarkably small ^{63,65}Cu hyperfine coupling ($60 < A_{zz} < 285$ MHz).[17,18,20]

The ligand field theory expression for the A_{zz} component of the ^{63,65}Cu hyperfine interaction is[20]

$$A_{zz} = P_d\left[-K\alpha^2 - \frac{4}{7}\alpha_2^2(a^2 - b^2) + \frac{(3a - 3^{1/2}b)\Delta g_{yy}}{14(a + 3^{1/2}b)} + \frac{(3a + 3^{1/2}b)\Delta g_{xx}}{14(a - 3^{1/2}b)} + \Delta g_{zz}\right] \quad (1)$$

where $P_d = g_e g_n \beta_e \beta_n \langle r^{-3}\rangle_d$ represents the usual dipolar interaction coefficient, α^2 represents the spin population in the Cu orbitals, and a and b are coefficients of $d_{x^2-y^2}$ and d_{z^2} in

Received: October 28, 2011
Published: March 20, 2012

   dx.doi.org/10.1021/ic202336m | *Inorg. Chem.* 2012, 51, 4066−4075

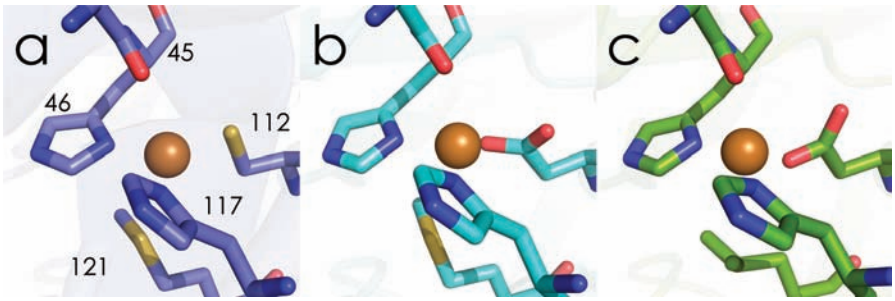

Figure 1. Substitutions to wild type azurin (a, PDBID: 4AZU) leading to type zero copper. The C112D variant (b, PDBID: 3FQY) binds type 2 Cu with essentially planar equatorial coordination. Removal of "south pole" axial ligation via M121L mutation gives rise to the pseudotetrahedral type zero site (c, PDBID: 3FPY). Oxygen atoms are red, nitrogen atoms are blue, and sulfur atoms are yellow.

the singly occupied molecular orbital (SOMO) that that leads to deviation from axial symmetry. Δg_{ii} ($i = x, y, z$) represents the shift of g_{ii} from the free electron value. Equation 1 consists of three contributions to A_{zz}:[20,21] (i) A_F, is the Fermi contact term ($-P_d K\alpha^2$) that is a consequence of spin population in Cu s orbitals (first term). (ii) A_S is the spin dipolar term that arises from a dipole−dipole interaction between the unpaired electron and nucleus (second term). (iii) A_L is the orbital dipolar contribution that is due to the interaction of nuclear spin with the magnetic field created by orbital angular momentum that constitutes all terms including Δg_{ii} (last three terms).

In the case of type 1 Cu^{II}, the small A_{zz} value has been ascribed to extensive delocalization of the SOMO over the ligands, particularly the thiolate sulfur, which reduces A_F and A_S.[20] A small A_{zz} value is also observed for Cu^{II} in a distorted tetrahedral geometry, such as in Cs_2CuCl_4. In this case, however, the small value is primarily a consequence of an increased A_L due to an increase in g_{zz}. As this contribution is opposite in sign to A_S and A_F, it leads to a reduction in A_{zz}.[20] The contribution of A_L is intimately related to the geometry of the Cu^{II} environment that determines its ground state as well as the positions of ligand field transitions.

The delocalized Cu−S bond combined with site rigidity conferred by outer-sphere hydrogen bonding interactions drastically reduces the ET reorganization energy from that of inorganic copper (type 1 copper $\lambda \sim 0.8$ eV).[22] The consensus emerging from a multitude of experimental and theoretical investigations is that the unique electronic properties of blue copper proteins require this very special type of thiolate ligation.

Copper sites with hard ligands and high- reduction potentials have been characterized in variants of the cupredoxin azurin from *Pseudomonas aeruginosa*.[23] Among these constructs were unexpectedly observed cases (C112D/M121X (X = L, F, I) azurins) featuring small A_{zz}(Cu) values, although they lack the thiolate ligand.[24] To distinguish these centers from well-established blue copper, they were called "type zero" sites. Importantly, type zero proteins exhibit enhanced ET activity, with low λ values, which was attributed to site rigidity conferred by the same hydrogen bond network found in wild-type azurin.[24,25]

In the present work, we explore the degree of covalency of type zero Cu^{II} sites through ligand hyperfine couplings arising from spin delocalization over the ligands, in an attempt to understand the origin of their small A_{zz}(Cu) values. Specifically, we compare the type zero copper site in azurin double mutants C112D/M121X (X = L, F) with the single C112D mutant that features normal type 2 behavior.[23] We have employed several complementary EPR (electron paramagnetic resonance) hyperfine spectroscopic techniques at X- and W-band (~9.5 and 95 GHz, respectively) frequencies to map the ligand hyperfine couplings. The hyperfine coupling of the coordinated histidine nitrogen atoms (^{14}N, ^{15}N) was determined from W-band ELDOR (electron−electron double resonance) detected NMR (ED-NMR), two-dimensional HYSCORE (hyperfine sublevel correlation) spectroscopy and ENDOR (electron−nuclear double resonance) spectroscopy. The hyperfine couplings of remote, weakly coupled nitrogen nuclei were determined using X-band HYSCORE and ^{13}C and ^{1}H hyperfine couplings using W-band ENDOR. Our results show that spin delocalization over the ligands in type zero Cu^{II} is different from that of type 2 Cu^{II} in the C112D mutant; the ^{14}N hyperfine couplings of the coordinated histidine nitrogens are smaller by about 25−40%, whereas that of the ^{13}C carboxylate of D112 is about 50% larger. We conclude that the reduced A_{zz}(Cu) value of type zero Cu^{II} is largely attributable to an increased orbital dipolar term, A_L, as a consequence of a distorted tetrahedral geometry. In addition, we suggest a relation between the increased spin delocalization on D112 carboxylate and the ET activity.

MATERIALS AND METHODS

All buffers were prepared with 18.2 MΩ Milli-Q water. Uniformly ^{13}C-labeled D-glucose and $^{15}NH_4Cl$ were purchased from Cambridge Isotopes.

Protein Synthesis and Purification. C112D and C112D/M121X (X = L, F) azurins were prepared as described previously.[23] Uniformly labeled C112D and C112D/M121X (X = L, F) were expressed using isotopically enriched M9 minimal media with a modified literature procedure.[25] Starter cultures of BL21(DE3) *E. coli* transformed with plasmids encoding the desired azurin were grown in 50 mL of LB containing 100 μg/mL of ampicillin inoculated from single colonies grown on LB/agar plates. These cultures were grown overnight with shaking at 37 °C. Cells were harvested through centrifugation at 5000 rpm with a Beckman JA-17 rotor for 10 min and resuspended in 20 mL of a fresh LB medium. A total of 10 mL of this suspension was used to inoculate 2 L of LB medium containing 50 μg/mL of ampicillin. This culture was grown with shaking at 37 °C until an OD_{600} of 0.8 was reached. At this point, the culture was pelleted by centrifugation at 3750*g* for 8 min. Cells were transferred into 2 × 4 L baffled Fernbach flasks, each containing 500 mL of minimal media made with $^{15}NH_4Cl$-containing M9 salts, 2 g of U−^{13}C glucose (Cambridge Isotopes), and 100 μg/mL of ampicillin. These cultures were grown with shaking at 37 °C for 1 h. The temperature was then

dx.doi.org/10.1021/ic202336m | *Inorg. Chem.* 2012, 51, 4066−4075

lowered to 32 °C. β-D-isopropylthiogalactopyranoside was added to 0.8 mM, and overexpression was then allowed to proceed for 7 h.

Cells were harvested by centrifugation at 3750*g* for 10 min. Cells were resuspended in 100 mL of a 20% sucrose solution containing 300 mM Tris (pH 8.1) and 1 mM EDTA and allowed to osmotically equilibrate for 45 min. Cells were then spun down at 7000 rpm for 20 min. Periplasmic extrusion was effected by resuspension in 30 mL of ice-cold 500 μM $MgCl_2$; the material was transferred to a 150 mL beaker with a magnetic stir bar and allowed to stir at 4 °C for 10 min. Contaminating nucleic acids were digested with DNase I and RNase A if the mixture became viscous. The material was then spun at 12 000 rpm in a Beckman JA-17 rotor for 30 min. Purification at this point followed the literature method,[24] although a Q FF FPLC column is substituted for the initial Q FF batch column. Purification on the Superdex 75 size-exclusion column was run with 50 mM HEPES pH 7.0 containing 150 mM NaCl. Proteins were reconstituted via the dropwise addition of 1.1 equivalents of $CuSO_4$ (100 mM stock in H_2O) to ∼1 mM apoprotein in 50 mM HEPES pH 7.0 buffer and subsequently desalting the protein via PD-10 column into experimental buffers.

Sample Preparation. H/D exchange was achieved via 1:1 (v/v) mixing of an H_2O prepared solution of azurin with 30% (v/v) glycerol-d_8 (Cambridge Isotopes Inc.) in D_2O. The resulting mixture was incubated for 1 day. The protein solutions were transferred into quartz capillaries (0.8 mm OD/0.6 mm ID for W-band, 3 mm OD for X-band), flash frozen, and stored in the liquid nitrogen. In order to prevent thawing, the capillary W-band samples were mounted into the EPR probe while immersed in a liquid nitrogen bath. Then, the cold probe, with the sample, was quickly transferred into the precooled cryostat. The UV absorption at 280 nm was used to determine the protein concentration resulting in [M121F] = 0.7 mM, [M121L] = 0.5 mM, and [C112D] = 1.5 mM for the enriched ^{13}C and ^{15}N samples. For the natural abundance samples, the concentrations were ∼2.0 mM.

Pulsed EPR Spectroscopy. W-band (95 GHz) measurements were performed on an in-house built spectrometer at 8 K,[26] and X-band pulsed EPR measurements were carried out on a Bruker ELEXSYS E580 spectrometer at 10 K. W-band echo detected EPR (ED-EPR) spectra were recorded using the two pulse echo sequence ($\pi/2-\tau-\pi-\tau-$echo) where all time intervals are kept constant and the magnetic field is swept. The microwave (MW) pulse lengths were $t_{\pi/2}$ =20 ns and t_π= 40 ns, and the interpulse delay, τ, was 550 ns.

W-band ENDOR spectra were measured using the Davies ENDOR pulse sequence,[27] $\pi-T-\pi/2-\tau-\pi-\tau-$echo, with a radiofrequency (RF) π pulse applied during the time interval T. For measurements of ^1H ENDOR spectra, the parameters were $t_{\pi/2}$ = 100 ns, t_π = 200 ns, τ = 400 ns, and t_{RF} = 25 μs; for ^{15}N and ^{13}C, $t_{\pi/2}$ = 100 ns, t_π = 200 ns, τ = 400 ns, and t_{RF} = 40 μs were used. The ^2H ENDOR spectra were measured using the Mims ENDOR sequence,[28] $\pi/2-\tau-\pi/2-T-\pi/2-\tau-$echo, with a RF pulse applied during the time interval T. The experimental conditions were $t_{\pi/2}$ = 20 ns, t_{RF} = 45 μs, and τ = 550 ns. This τ value places the blind spots well outside the spectral range. In the ENDOR experiments, the echo intensity is measured as a function of the RF pulse frequency. All ENDOR spectra were recorded using the random acquisition mode,[29] with one shot for each point, and the total number of scans was varied in the range 100−1500 depending on the S/N. The overall repetition time was 13−14 ms, which includes the instrumental overhead stemming from the time required for the data transfer from ADC to SpecMan program and variations of the time intervals and the RF.[30]

W-band ED-NMR[31] was measured with the pulse sequence $t_{pump}-t-\pi_{obs}/2-\tau-\pi_{obs}-$echo, where the subscripts pump and obs indicate different microwave frequencies. In this experiment, the frequency of the observer (obs) pulses is fixed at ν_1, and the frequency of the pump pulse, ν_2, is varied. The spectra are presented using the scale of $\Delta\nu = \nu_1 - \nu_2$. The lengths of the $\pi_{obs}/2$ and π_{obs} pulses were 100 and 200 ns, respectively; τ was equal to 400 ns. The microwave field strength of the pump pulse was ∼2.5 MHz (for $\Delta\nu = 0$), which for a t_{pump} pulse of 10 μs yields a nominal flip angle of 5π.

W-band HYSCORE[32] spectra were measured with the $\pi/2-\tau-\pi/2-t_1-\pi-t_2-\pi/2-\tau-$echo sequence where t_1 and t_2 are varied and echo intensity is monitored. A four-step phase cycle has been used to remove unwanted echoes.[33] The lengths of the $\pi/2$ and π pulses were 12.5 and 25 ns respectively; the length of interval τ is given in the figure captions. The starting value for t_1 and t_2 was 50 ns, and it was incremented in 12.5 ns steps to obtain a 90 × 90 data set. Background decay was removed by subtracting a second order polynomial, the resulting data were apodized by a Gaussian function in both dimensions, zero filled to 256 points, and 2D fast Fourier transformed to obtain the final spectra, shown in magnitude mode.

X-band HYSCORE was carried out with the same sequence used for W-band HYSCORE measurements with $\pi/2$ and π pulses of 12 and 24 ns, respectively. t_1 and t_2 were incremented in 48 ns steps; 128 points were collected in each dimension. The length of interval τ is given in the figure captions. The data were treated as described for the W-band HYSCORE spectra.

In the following, we give a brief description of the ^{14}N frequencies observed in spectra recorded with the above methods and their relation to the spin Hamiltonian parameters. There are three nuclear frequencies within each of the α (M_S = 1/2) and the β (M_S = −1/2) electron spin manifolds, ν_{sq1}^{α}, ν_{sq2}^{α}, and ν_{dq}^{α} and ν_{sq1}^{β}, ν_{sq2}^{β}, and ν_{dq}^{β}, respectively. The notation sq corresponds to single quantum transitions and dq to double quantum transitions. To first order

$$\nu_{sq1,2}^{\alpha} = \nu_{14N} - A(\theta, \phi)/2 \pm P(\theta, \phi) \quad (2)$$

$$\nu_{sq1,2}^{\beta} = \nu_{14N} + A(\theta, \phi)/2 \pm P(\theta, \phi) \quad (3)$$

where ν_{14N} is the ^{14}N Larmor frequency and $A(\theta,\phi)$ and $P(\theta,\phi)$ are the hyperfine and nuclear quadrupole couplings that depend on the orientation (θ,ϕ) of the magnetic field with respect to the molecular axes system. For I = 1/2 nuclei, like ^{13}C, ^{15}N, and ^1H, $P(\theta,\phi) = 0$, and there is only one nuclear transition per electron spin manifold.

HYSCORE is a two-dimensional correlation experiment where cross-peaks appear between nuclear frequencies belonging to different electron spin manifolds, namely, ($\nu_{sq1,2}^{\alpha}$, $\nu_{sq1,2}^{\beta}$), ($\nu_{sq1,2}^{\alpha}$, ν_{dq}^{β}), and (ν_{dq}^{α}, ν_{dq}^{β}) and their symmetric counterparts. W-band HYSCORE is particularly useful for observing ^{14}N hyperfine couplings around 20 MHz, which at W-band are within the cancellation condition, $|A| \sim 2\nu_{14N}$.[34,34] X-band HYSCORE is effective for smaller hyperfine couplings.

dx.doi.org/10.1021/ic202336m | Inorg. Chem. 2012, 51, 4066−4075

RESULTS

The W-band echo detected (ED) EPR spectra of the three azurin mutants studied in this work are shown in Figure 2. The

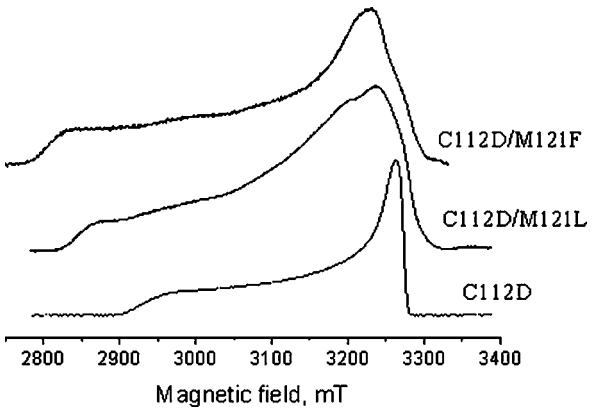

Figure 2. W-band echo detected EPR spectra of C112D and C112D/M121X (X = L, F) azurins.

g values extracted from their apparent features in the spectrum are presented in Table 1. Generally they agree well with those

Table 1. Copper Site g-Values of the Azurin Mutants Measured at W-Band Compared with the X-Band Reported Values[24]

	g_{xx}, g_{yy}, g_{zz} (W-band)[a]	g_{xx}, g_{yy}, g_{zz} (X-band)
C112D	2.08, 2.08, 2.31	2.063, 2.063, 2.311
C112D/M121L	2.07, 2.10, 2.38	2.04, 2.116, 2.381
C112D/M121F	2.07, 2.09, 2.41	2.054, 2.10, 2.386

[a]The estimated error in the W-band g value is ±0.005.

determined from continuous wave (CW) X-band spectra,[24] and the small differences are attributed to the increased line width of the W-band spectra due to unresolved ^{63,65}Cu hyperfine couplings and g strain. Small inaccuracies in the W-band field sweep will also contribute. The rhombicity of **g** of the double mutants, C112D/M121X (X = F, L), is well resolved and is in strong contrast to the axial symmetry of the single mutant, C112D. The spectra of the double mutants show some wiggles that are attributed to nuclear modulations, the depth of which varies with the magnetic field.[35]

^{14}N Hyperfine Couplings of the Coordinated Nitrogens. The hyperfine couplings of the coordinated ^{14}N were first probed by W-band ED-NMR. Figure 3a shows a series of ED-NMR spectra of the C112D mutant recorded at several field positions within the EPR spectrum. The spectrum measured at 3289 mT ($g_\perp$) resolves two pairs of lines, at 4.2 ± 0.3 and 8.6 ± 0.3 MHz and at 23.7 ± 0.5 and 28.3 ± 0.5 MHz. At this field, the ^{14}N Larmor frequency, ν_{14N}, is 10.17 MHz, and there are two possible assignments for these lines. One possibility is that all four signals belong to one type of nucleus where all four $\nu_{sq1,2}^{\alpha,\beta}$ lines are well resolved, yielding A = 32.4 ± 1.1 MHz and P = 2.2 ± 1.1 MHz (eqs 2 and 3). Thus, for this case, the N_δ's of H46 and H117 have the same hyperfine and quadrupole couplings. The second possibility is that these lines belong to two nuclei, N_1 and N_2, with different hyperfine couplings and unresolved quadrupolar splitting: for N_1, $A_1(^{14}N)$ = 27.9 ± 0.8 MHz (the 4.2 and 23.7 MHz lines, marked with ○ on Figure 3a), and for N_2, $A_2(^{14}N)$ = 36.9 ± 0.8 MHz (the 8.6 and 28.3 MHz lines, marked with * in Figure 3a). Namely, N_δ's of H46 and H117 have different hyperfine couplings.

To distinguish between these two alternatives, we have carried out ED-NMR and ENDOR measurements on a ^{15}N, ^{13}C enriched C112D sample. Since ^{15}N has I = 1/2 and therefore does not have a quadrupolar moment, the two cases can easily be distinguished (see Figure S1 in the Supporting Information (SI) and explanations therein). The spectra obtained clearly support option two and exclude option one. Further support for this assignment was provided from W-band HYSCORE measurements.

The HYSCORE spectrum, recorded at $g_\perp$ and shown in Figure 4a, has one type of cross peak in the (−,+) quadrant at (∼−5, ∼24) MHz (and the symmetric counterpart (∼−24,∼5)) MHz, consistent with the assignment of these

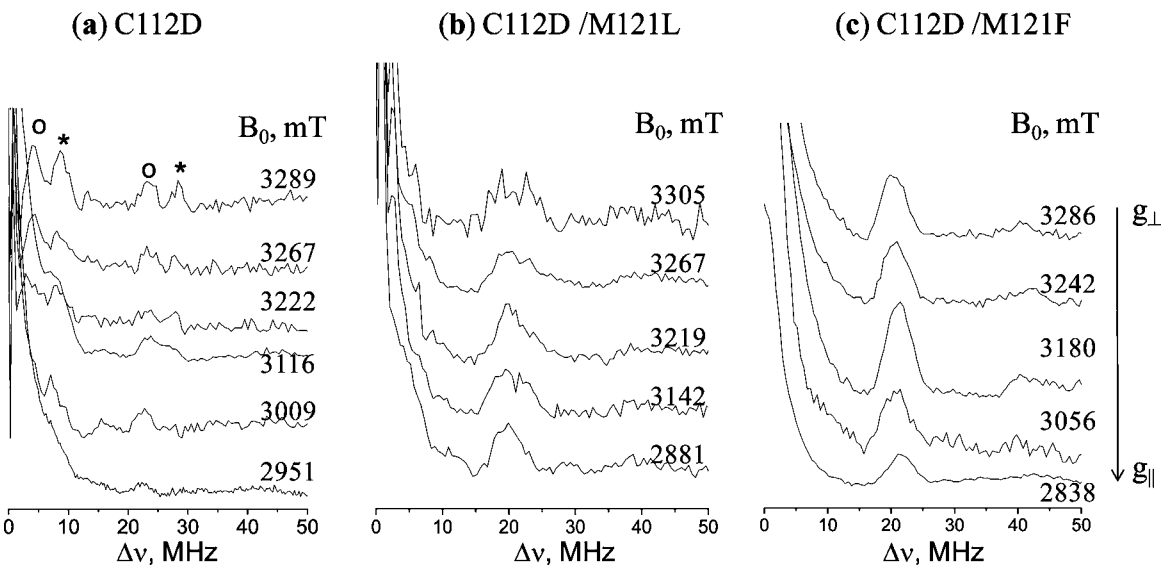

Figure 3. ED-NMR spectra of natural abundance (a) C112D, (b) C112D/M121L, and (c) C112D/M121F azurins measured at different magnetic field strengths through the EPR spectra. The symbols ○ and * mark the peaks assigned to N_1 and N_2, respectively.

dx.doi.org/10.1021/ic202336m | Inorg. Chem. 2012, 51, 4066−4075

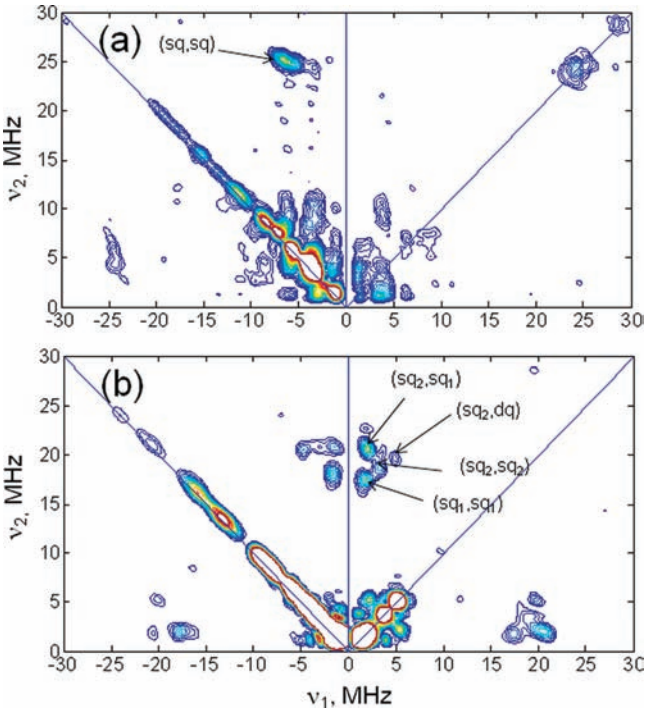

Figure 4. W-band HYSCORE spectra of (a) C112D azurin measured at 3289 mT with τ = 137.5 ns and (b) C112D/M121F azurin recorded at B = 3242 mT and τ = 250 ns. The strong signals on the diagonal of the (−,+) quadrant arise from the primary echo overlapping with the stimulated echo when $t_1 = t_2$ in HYSCORE sequence, which was not removed **completely** by the employed phase cycle.

lines to N_1. We could not observe any cross peaks involving the 28 MHz signal of N_2, although it does appear on the (+,+) diagonal. Such cross peaks are associated with a hyperfine coupling that is farther from the cancellation condition ($A \sim 2\nu_{14N}$),[36] and therefore their intensity is expected to be lower. Moreover, due to MW power limitations, the bandwidths of the MW pulses are insufficient to excite both the allowed and forbidden transitions as required for this experiment. In an earlier work on ascorbate oxidase, Goldfarb and co-workers[34] determined that $A > 0$ for the directly bound nitrogen in type 2 Cu^{II}, and therefore we assign the low frequency signals to the α manifold. The cross peaks observed, and their assignments are listed in Table 2.

The field dependence of the ED-NMR spectrum, presented in Figure 3a, shows that as the observer field decreases, there is some change in peak frequencies, particularly those belonging to N_1, which decrease as the field decreases. At lower fields, close to $g_{\|}$, the quality of the spectra is low; nonetheless, peaks at 7 MHz, assigned to N_2, and at 22.5 MHz, assigned to N_1, are clear. We estimate from them $A_{2,min}(^{14}N)$ = 32 ± 1 MHz and $A_{1,min}(^{14}N)$ = 27 ± 1 MHz. This indicates some finite anisotropy for $^{14}N_2$, of about 4 MHz, and only ∼1 MHz for $^{14}N_1$.

Table 2. The Assignment and Frequencies (MHz) Observed in the W-Band HYSCORE Spectra of C112D and C112D/M121X (X = L, F) Azurins

	X = F	X = L	C112D
(ν_{sq1}^{β}, ν_{sq1}^{α})	[(17.5–18, 1.5–1.7)][a]	[18, (1.5–2)]	[(24–25), (2–7)]
(ν_{sq2}^{β}, ν_{sq1}^{α})	[(19.6–21), (1.5–1.7)]	[(20–23), (1.5–2)]	
(ν_{sq2}^{β}, ν_{sq2}^{α})	[19.5, 3.5]	[(20–23), 3.5]	
(ν_{sq2}^{β}, ν_{dq}^{α})	[(19.2–21), (4.8–5)]	[(20–23), (4.5–5)]	

[a]Because of the powder characteristics of the sample, particularly when the experiment is carried out at g_{yy} where many molecular orientations contribute to the signal, a range of individual frequencies that cover the range of frequencies spanned by the different cross peaks is given.

The ED-NMR spectra of C112D/M121L azurin recorded at several fields along the EPR spectrum are depicted in Figure 3b. The spectra show a broad line around 20 MHz and a shoulder at ∼5 MHz. The field dependence is mild and is manifested mainly in a line narrowing toward low fields (g_{zz} position). The ED-NMR and ENDOR spectra of the $^{15}N/^{13}C$ sample (Figure S2) exhibited two lines at 27 and 34 MHz showing that also for C112D/M121L the two coordinated histidine ^{14}N nuclei are inequivalent with $A_1(^{14}N)$ = 18.5 ± 1 MHz and $A_2(^{14}N)$ = 27 ± 1 MHz. The low frequency component of the ^{14}N doublet was clearly observed in the HYSCORE spectrum. The spectrum is generally similar to that of C112D, with rather broad cross peaks around (−4, 20) MHz in the (−,+) quadrant (Figure S3), not resolving the two nitrogens. This is consistent with the ED-NMR spectra. Spectra measured also at g_{zz} were better resolved, but no significant shifts were observed (not shown).

The ED-NMR spectra of C112D/M121F azurin exhibit a single peak at 20 MHz and a weak signal at 40 MHz assigned to the double quantum frequency ν_{dq}^{β}. Here, the low frequency peak of the doublet is not resolved. From the 20 MHz signal, we obtain $A_1 = A_2 \sim 20 \pm 0.5$ MHz. The position of the ^{14}N line does not vary with the magnetic field, indicating that the hyperfine anisotropy is negligible. A W-band HYSCORE spectrum of C112D/M121F azurin, recorded at the g_{yy} position (3242 mT), is shown in Figure 4b. (Spectra recorded under different conditions are shown in Figure S4.) A number of cross peaks appear in both (+,+) and (−,+) quadrants. The frequencies of the peaks and their assignments are listed in Table 2. The frequencies of $\nu_{sq1,2}^{\beta}$ are in good agreement with those observed in the ED-NMR spectrum (Figure 3c), and their resolution allows for estimating the quadrupolar splitting $2P \sim 2.5$ MHz. As in the ED-NMR spectra, the signals of the N_{ε} of the two different histidines are not resolved. The observed frequencies are summarized in Table 2 as well. Table 3 lists the ^{14}N hyperfine couplings of the three mutants, derived from all of these measurements.

^{13}C Hyperfine Couplings. To further characterize the ligands of type zero Cu^{II}, we carried out W-band ENDOR measurements on $^{15}N/^{13}C$ enriched samples, focusing on the ^{13}C region. Figure 5 shows the W-band Davies ENDOR of $^{15}N/^{13}C$ enriched samples of C112D and C112D/M121X (X = L, F) azurins measured at the position of maximum signal ($g_{\perp}$, g_{yy}, respectively). The spectra consist of several doublets centered around the Larmor frequency of ^{13}C, ν_{13C}, that reveal again marked differences between the C112D and C112D/M121X (X = L, F) azurins. The largest hyperfine coupling observed in the ENDOR spectrum of C112D is ∼5 MHz, and a spectrum recorded at 3222 mT (see Figure S5) resolved two doublets with 3.8 and 6.2 MHz splitting. Unfortunately, due to S/N limitations, we were not able to record a full series of orientation selective spectra for any of the samples. The C112D/M121X (X = L, F) mutants have rather similar spectra, with a largest splitting of ∼9 MHz. It is difficult, however, to assign all of the observed couplings to any particular nucleus.

dx.doi.org/10.1021/ic202336m | Inorg. Chem. 2012, 51, 4066–4075

Table 3. Summary of the Hyperfine Couplings (in MHz) Obtained for the Azurin Mutants Studied by Pulsed EPR Compared with Literature Values for WT Azurin and DFT Calculated Values (designated by the superscript cal)[52]

nucleus	C112D	C112D/M121L	C112D/M121F	WT
^{14}N (His)−direct	$A_{1,max}$ = 27.9 ± 0.8	A_1 = 18.5 ± 1	A_1= A_2 = 20 ± 0.5	(19.1, 18.0, 17.2) H46[41]
	$A_{1,min}$ = 27 ± 1	A_2 = 27 ± 1		A_{iso}=*18.1*
	$A_{2,max}$ = 36.9 ± 0.8			(27.8, 24.0, 23.6) H117[41]
	$A_{2,min}$ = 32 ± 1			A_{iso}= *25.1*
	A_{iso}^{cal} (*H46*) = 37	A_{iso}^{cal} (*H46*) = 22	A_{iso}^{cal} (*H46*) = 19.9	A_{iso}^{cal} (*H46*) = 19.8
	A_{iso}^{cal} (*H117*) = 26.3	A_{iso}^{cal} (*H117*) = 3.15	A_{iso}^{cal} (*H117*) = 17	A_{iso}^{cal} (*H117*) = 27.2
^{13}C−(OC)	|*A*| ∼ 5.8 ± 0.4	|*A*| ∼ 9 ± 1	|*A*| ∼ 9 ± 1	
	A_{iso}^{cal} (*D112C*$_\gamma$) = −5.64	A_{iso}^{cal} (*D112C*$_\gamma$) = 6.9	A_{iso}^{cal} (*D112C*$_\gamma$) = −9	
^{14}N (His)−remote	A_a ∼ 1.5	A_a = 1.4−1.6	A_a = 1.3−1.4	A_{iso} = 1.3 (H117)[42]
	A_b = 1.7−1.8	A_b = 1.8−1.9	A_b = 1.7−1.9	A_{iso} = 0.87 (H46)[42]
	A_{iso}^{cal} (*H46*) = 1.81	A_{iso}^{cal} (*H46*) = 1.74	A_{iso}^{cal} (*H46*) = 1.58	A_{iso}^{cal} (*H46*) = 0.83
	A_{iso}^{cal} (*H117*) = 1.35	A_{iso}^{cal} (*H117*) = 0.54	A_{iso}^{cal} (*H117*) = 1.7	A_{iso}^{cal} (*H117*) = 1.37

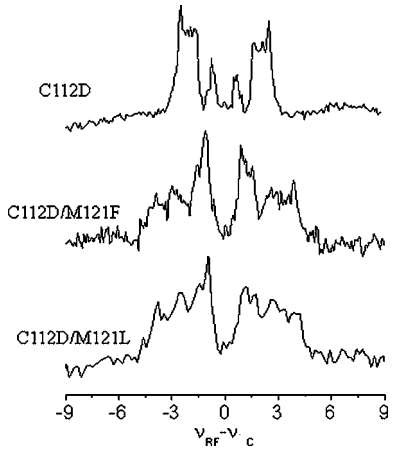

Figure 5. W-band Davies ENDOR of ^{15}N/^{13}C enriched C112D and C112D/M121X (X = L, F) measured at the position of maximum signal (g_{yy}, $g_\perp$, respectively).

Nonetheless, considering that the ^{14}N hyperfine couplings of the coordinated nitrogens are larger in C112D, it is unlikely that the large ^{13}C couplings arise from the histidines. Therefore, we tentatively assign the 9 MHz splitting to D112C$_\gamma$. This will be discussed further later.

^{14}N Hyperfine Couplings of the Remote Nitrogens. In order to detect any weakly coupled ^{14}N nuclei such as the remote N$_\varepsilon$ of the histidine ligands or the backbone ^{14}N's of G45 or D112, we have also performed X-band HYSCORE measurements. These are known to be particularly useful for the detection of remote nitrogens in the Cu^{II} coordination sphere.[37] The HYSCORE spectra of the three mutants recorded at maximum echo intensity ($g_\perp$ for C112D and g_{yy} for the other two) are shown in Figure 6. All three spectra are rather similar, showing a set of three cross peaks of the type ($\nu_{sq1,sq2,dq}^{\alpha}$, ν_{dq}^{β}) (assuming $A > 0$) where two remote nitrogens can be resolved. Table S1 summarizes the frequencies of all peaks observed and their assignments. From these spectra, we estimate A_a(^{14}N) = 1.7−1.9 MHz and A_b(^{14}N) = 1.3−1.6 MHz, a quadrupole coupling constant, e^2Qq/h ∼1.51 MHz, and an asymmetry parameter, η ∼ 1, and assign them to two histidine remote nitrogens. It is interesting to note that while significant differences between the couplings of the directly coordinated ^{14}N were observed between the C112D mutant and the C112D/M121X (X = F, L) mutants, these differences could not be resolved in the remote nitrogens. The hyperfine and

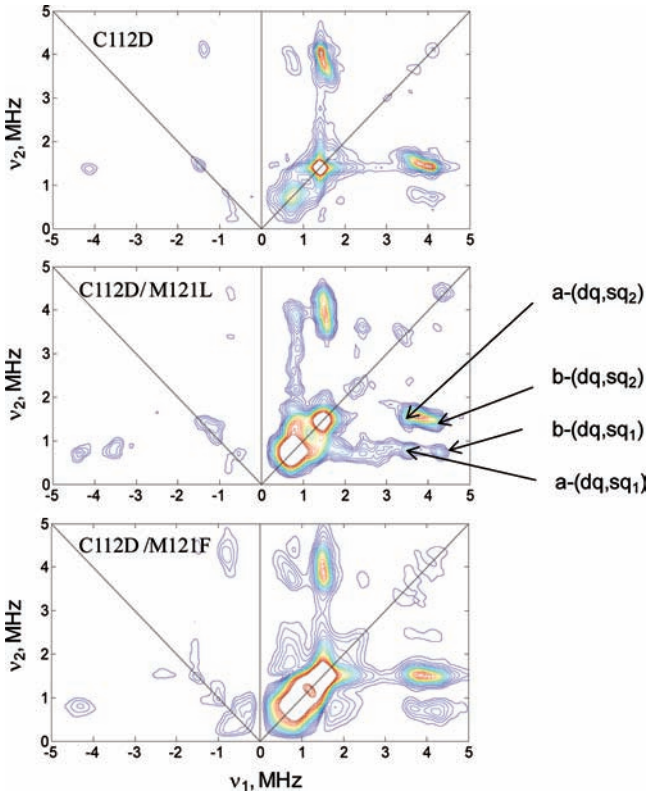

Figure 6. X-band HYSCORE spectra of the three mutants recorded at 330 mT.

quadrupole parameters obtained are well within the range observed for histidine remote nitrogens in type 1 and type 2 Cu^{II} in other proteins.[38] In fact, the HYSCORE spectra are very similar to that of wild type (WT) azurin[37] except that it lacks the cross peaks arising from a backbone ^{14}N assigned to C112.[39] To conclude, these measurements did not detect any spin density from the G45 backbone ^{14}N or any other weakly coupled backbone nitrogen as observed for WT azurin. Table 3 lists all hyperfine couplings determined for the mutants studied, compared with the corresponding couplings of WT azurin when available.

^{1}H Hyperfine Couplings. To complete the picture of the spin density delocalization in type zero Cu^{II}, we have measured ^{1}H ENDOR spectra, searching for unusually large hyperfine couplings, beyond those expected from the point-dipole approximation, that may indicate some large spin density on

dx.doi.org/10.1021/ic202336m | *Inorg. Chem.* 2012, 51, 4066−4075

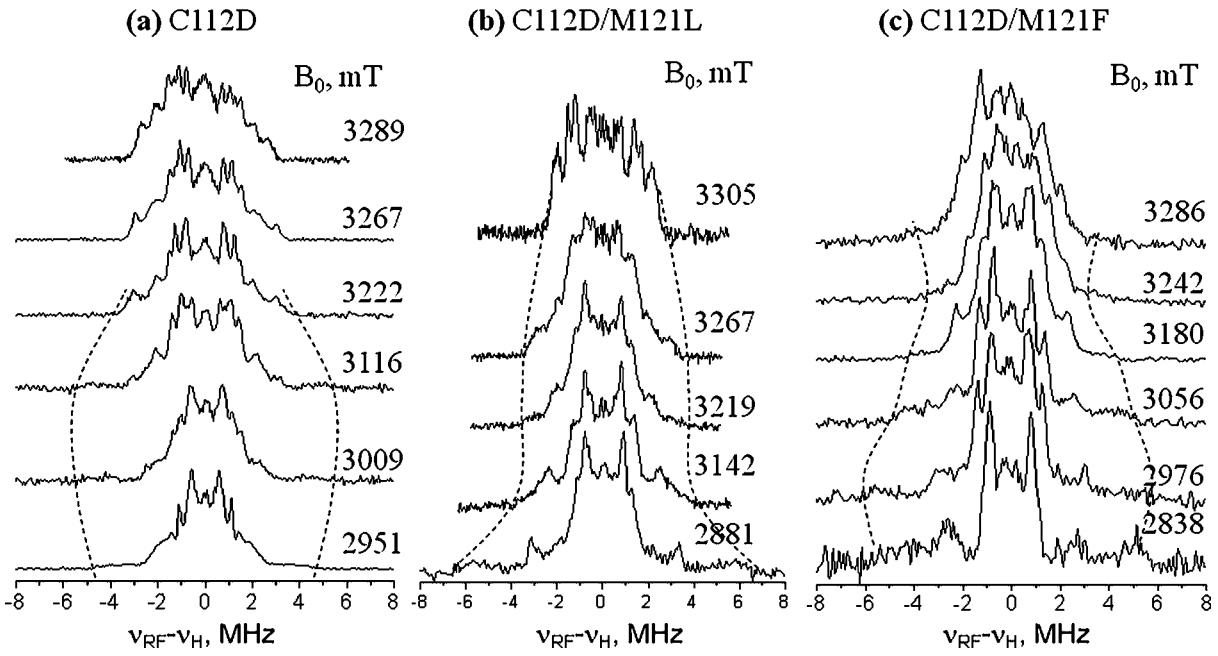

Figure 7. W-band ^{1}H Davies ENDOR spectra of the C112D (a), C112D/M121L (b), and C112D/M121F (c) azurins measured at different magnetic fields within the EPR spectrum. The dotted lines trace the largest couplings.

the ligands. The largest couplings, $A_{\|}(^{1}H) \sim 11-12$ MHz, are observed for the type zero double mutants in the region of g_{zz} (see Figure 7b,c). In contrast, for C112D, the maximum splitting, ~12 MHz, is observed for magnetic fields in the center of the powder pattern (see Figure 7a). The multitude of protons renders assignment difficult. Therefore, we estimated the dipolar interaction from the crystal structures of C112D and C112D/M121L with added hydrogens using the point dipole approximation, and the results are listed in Table S2. This was calculated for 100% spin density on the Cu^{II}. The actual spin density is lower, and therefore the calculated couplings may be overestimated by about 20−30%.

The most likely candidate for the closest proton with the largest dipolar coupling is the proton attached to C_{α} of H46. It gives $A_{\|} \sim 12$ MHz and $A_{\|} = 11.3$ MHz for C112D/M121L and C112D, respectively. Signal assignments may be facilitated by identifying water exchangeable protons. To this end, ENDOR spectra were measured using samples partially enriched with D_2O (Figure S6). The spectra of both samples reveal the disappearance of lines at ±2 MHz (largest coupling) upon the addition of D_2O, which can be identified in the corresponding ^{2}H ENDOR spectra. The dipolar couplings derived from the crystal structure did not reveal any obvious candidate for these exchangeable protons (Table S1). DFT calculation gave for the optimized structures of C112D/M121L and C112D a finite isotropic hyperfine constants around 1.5 MHz and 0.6−0.9 MHz for the exchangeable ring proton $H_{\varepsilon 2}$ of H46 and H117, respectively.[52] Thus, this coupling could arise from the H46 ring. The proton couplings observed do not deviate significantly from those expected from dipolar interactions and do not reveal any large unexpected spin density that would be manifested by a large isotropic hyperfine coupling as observed for the cysteine β-protons in type 1 copper.[40] In addition, no significant differences were observed in the maximum width of the spectra between single and double mutants. The spectra of the two C112D/M121L/F mutants are rather similar, while they differ considerably from C112D in terms of their field dependence but not total width. This should be a consequence of their different ligands' orientation relative to the g principal axes system.

DISCUSSION

Using a number of hyperfine spectroscopy techniques, applied at W- and X-band frequencies, we were able to map the ligand hyperfine couplings of the type 2 Cu^{II} center in the single C112D mutant of azurin and the new type zero Cu^{II} in C112D/M121X (X = L, F; see Table 3). Employing a combination of complementary techniques, mostly carried out at W-band, together with isotopic labeling, we were able to observe and assign the nuclear frequencies of first and second shell ligands. Measurements at high field were essential to resolving the nuclear frequencies of the different nuclei, particularly by moving the proton signals to much higher frequencies. W-band ED-NMR of the directly coordinated ^{14}N nuclei was found to have the best sensitivity, and signals could be measured also at the $g_{\|}$ (g_{zz}) region. High field ED-NMR emerges as a very efficient way to record nuclear frequencies of strongly coupled low γ quadrupolar nuclei such as ^{14}N and ^{17}O.[34,43−48] Here, the sensitivity increases when the cancellation condition is met ($|A| \sim 2\nu_I$),[34,34] namely, for ^{14}N with $A \sim 20$ MHz. Under these conditions, the intensity of the EPR "forbidden transitions", essential for the observation of ED-NMR, is the highest. In this case, we were also able to observe the double quantum transition ν_{dq}^{β} at ~40 MHz. In some of the ED-NMR spectra, however, it was difficult to resolve the low frequency components because they were masked by the broad central, $\Delta\nu = 0$ line. These low frequencies were readily detected in the W-band HYSCORE spectra, which could resolve quadrupolar splittings.[34] In cases where there were contributions from more than a single ^{14}N nucleus, e.g., the C112D mutant, the cross peaks in the HYSCORE spectra helped correlating the signals observed to a particular ^{14}N nucleus. The HYSCORE signals, similar to the ED-NMR ones, have the highest intensity when the cancellation condition

dx.doi.org/10.1021/ic202336m | Inorg. Chem. 2012, 51, 4066−4075

holds. The limitation of W-band HYSCORE on our spectrometer is A(^{14}N) <30 MHz because both the limited bandwidth of the inversion pulse and the deviation from the cancellation condition reduce the sensitivity. Finally, for S=1/2 nuclei, such as ^{1}H, ^{13}C and ^{15}N W-band ENDOR gave the best results because the intensity of the forbidden EPR transitions is low. This is due to the lack of a quadrupolar interaction that increases the probability of the forbidden EPR transitions by enhancing the mixing of the nuclear states.

The ^{14}N hyperfine couplings of the directly coordinated histidine ligands of the Cu^{II} type 2 in C112D are generally larger than those of the wild type (see Table 3). This is consistent with the larger hyperfine couplings (around 40 MHz) generally observed for Cu^{II} type 2.[49,50] While $A(^{14}N_2)$ is within this range, $A(^{14}N_1)$ is significantly smaller. Considering that the hyperfine couplings in tetragonal Cu^{II} originate from overlap between the sp^2 orbital of the nitrogen and the lobe of the Cu^{II} $(x^2 - y^2)$ orbital, which is the ground state for type 2 Cu^{II},[51] this suggests that N_1 deviates from the equatorial plain in C112D. If we follow the qualitative approach of Hoffman and co-workers[51] and take the ^{14}N hyperfine coupling of Cu(imidazole)$_4$, 40−42 MHz, as a reference for imidazole coordinated to Cu^{II} in an unconstrained square-planar complex with a spin density, ρ_N, of 0.09, we obtain $\rho_{N1} \sim 0.06$ and $\rho_{N2} \sim 0.08$. Here, we neglected the anisotropic hyperfine contributions, which were resolved only for C112D and were rather small. This compares quite well with the Löwdin spin populations obtained from density functional theory (DFT) calculations of C112D, 0.071 for H46 and 0.055 for H117.[52] The histidines' $A(^{14}N)$ values of the type zero Cu^{II} in C112D/M121X (X = L, F) are closer to those of WT azurin, and using the above arguments we obtain for X = L $\rho_{N1} \sim 0.06$ and $\rho_{N2} \sim 0.04$ and for X = F $\rho_{N1} \sim \rho_{N2} \sim 0.04$. The predicted DFT values[52] are $\rho_N = 0.05$ and 0.013 for X = L and $\rho_N = 0.047$ and 0.040 for X = F, for H46 and H117, respectively. Again the values compare well with DFT ones, except for H117 of C112D/M121L. The ^{14}N isotropic hyperfine values, A_{iso}, of the coordinated N_δ and remote N_ε obtained from the DFT calculations[52] are listed in Table 3 and compared with experimentally determined ones. The agreement for C112D is remarkable and for C112D/M121F is very good. We also found agreement for the H46 nitrogen nuclei of C112D/M121L but not for those of H117. The disagreement for H117 may be an artifact of the geometry sensitivity of the calculations.

The first coordination shell ligands that have to be considered next are the D112 carboxylate for all three mutants and the backbone oxygen of G45 for the double mutants. These were probed via ^{13}C ENDOR of the carbon coordinated to first shell oxygen ligands. Here, we assigned the largest ^{13}C hyperfine coupling observed in the C112D/M121X (X = L, F) mutants to D112C$_\gamma$ and not to one of the histidine carbons, on the basis of a comparison with C112D couplings. As the histidine ^{14}N hyperfine couplings are larger in C112D than in type zero mutants, we expect that the ^{13}C hyperfine coupling of the next nearest neighbors will be larger as well. In contrast, both type zero mutants exhibit larger couplings. We exclude the possible assignment of the 9 MHz ^{13}C hyperfine coupling to the backbone carbon of G45 because of the larger Cu−O distance[23] and the lack of any signals from a weakly coupled backbone nitrogen, as found in azurin.[13,37] Support for this assignment is obtained also from the DFT calculations[52] that predicted relatively large couplings for D112C$_\gamma$ (see Table 3). Because we were not able to record a full set of orientation selective ^{13}C ENDOR spectra, we cannot unambiguously state that the 6 MHz coupling observed for C112D is indeed the largest coupling. However, since the carboxylate is in the equatorial plane, it is highly probable that by aligning the field along $g_\perp$ we should observe the largest couplings.[53] The very good agreement between the DFT predicted values[52] (Table 3) and the experimental ones supports this assumption. Excellent agreement also was obtained for C112D/M121F, but it was only satisfactory for C112D/M121L.

In Table 4, we have collected a series of reported ^{13}C hyperfine couplings for model Cu^{II} complexes and of carboxyl radicals, $CO_2^{\bullet-}$, given for comparison. The latter, where practically all the spin is situated on the carbon atom,[54] indicates that the ρ_c of D112C$_\gamma$ in C112D/M121X (X = L, F) does not exceed 2%. For all of the Cu^{II} complexes involving oxygen coordination listed in Table 4, the ^{13}C hyperfine tensor is rhombic, indicating a significant spin population in the carbon p_z orbital. Unfortunately, we could not obtain all three principal hyperfine components that would allow estimating the p_z spin population. Nonetheless, the 9 MHz coupling observed for the type zero mutants is on the high side of those listed for oxygen ligands in Table 4 and is close to the values of carboxylate bidendate coordination. In this model compound, the direction of $A_3 = 9.0$ MHz is tilted by 75° ± 5° with respect to the $g_\parallel$. This is in agreement with the observation of 9 MHz coupling in the type zero mutants along the g_{yy} direction. This would suggest bidentate coordination of the D112 carboxylate, which does not accord with the crystal structure[23] nor the DFT calculations.[52] Moreover, the participation of the noncoordinating oxygen of D112 in H-bonding with the amide protons of N47 and F114 was marked as crucial for the restoration of the hydrogen-bond network that enhances the ET reactivity of type zero copper over that of the type 2 C112D mutant.[25] Therefore, we exclude the possibility of bidentate coordination.

^{13}C hyperfine couplings as large as −9 to −10 MHz were observed in Cu^{II} complexes with dichalcogenide ligands.[55] Here, a large negative isotropic hyperfine is generally observed and is attributed to spin polarization. In these complexes, the unpaired electron occupies a molecular orbital that consists mainly of the Cu $3d_{xy}$ orbital and the corresponding 3s and 3p orbitals of the sulfur donors. Consequently, the spin-density on the sulfur has a positive sign and the mechanism that results in

Table 4. The ^{13}C Principal Hyperfine Components in Cu^{II} Model Complexes

compound	^{13}C position	hyperfine couplings, MHz	ref
$CO_2^{\bullet-}$	$^{13}CO_2^{\bullet-}$	A_{iso} = 409−426	54
Cu−histidine (pH = 3.8)	carboxylate	−1.9, −3.5, −5.7	58
Cu−glycine	carboxylate	−1.4, −3.5, −5	58
Cu carbonate	bidentate	4.0, 6.9, 9.0	53
Cu carbonate	monodentate	0.1, 0.1, 3.5	53
Cu−Zn acetate dimer	the largest carboxylate hyperfine out of four	0.63 −4.10 −4.8	40
Cu−bis(diethyl-dithiocarbamate doped in Zn crystals	the ^{13}C with the largest coupling	−8.46 −9.96 −10.2	59, 55
Cu−bis(diethyl-dithiocarbamate doped in Ni crystals	the ^{13}C with the largest coupling	−6.69 −8.16 −9.36	60, 55
tetra-N-butylammonium-bis-(maleonitrile-dithiolato)Cu(II)	the ^{13}C with the largest coupling	−3.1 −3.59 −5.25	55

dx.doi.org/10.1021/ic202336m | Inorg. Chem. 2012, 51, 4066−4075

a spin population in the next-neighbor s orbitals was attributed to spin polarization.[55] The spin density on the oxygen in the type zero sites, being a harder ligand, is expected to be lower than that on the sulfur, and therefore the similar ^{13}C hyperfine coupling is surprising. This suggests elevated spin population on D112O$_{\varepsilon 1}$. DFT calculations predicted spin populations of 15% (X = F) and 10.8% (X = L) for D112O$_{\varepsilon 1}$ of C112D/M121X.[52] The values obtained for C112D in bidentate coordination that fit spectroscopic experimental data are 10.2% and 9.1%.[52] However, substantial spin population was not found by DFT further along the D112 side chain in the C112D protein. In type zero proteins, interestingly, spin population delocalized to a greater extent along the D112 side chain, suggesting enhanced coupling between the protein and Cu in these active centers.[52]

The ^{1}H ENDOR spectra do not show unusually large hyperfine couplings, and the largest couplings observed in all three mutants are similar. This is consistent with the assignment of the largest ^{13}C hyperfine coupling in C112D/M121X (X = L, F) to D112C$_{\gamma}$, where the closest protons would be on C$_{\beta}$. These protons are quite far from the Cu^{II} and the coordinated oxygen, and therefore the couplings are small although the spin density on the oxygen may be significant. The alternative assignment of $A(^{13}C) \sim 9$ MHz to a carbon in one of the histidine ligands is expected to lead to larger ^{1}H couplings, which is not observed.

The qualitative analysis of all hyperfine couplings presented in this work, and the comparison between the C112D and C112D/M121X (X = L, F) proteins, show that the spin delocalization over the histidine ligands for type zero Cu^{II} is similar to that of WT, and lower than in C112D. In contrast, larger spin density is found on the equatorial D112 ligand of type zero in the double mutants compared to type 2 in C112D. This increase on its own, however, is not large enough to account for the low Cu A_{zz} value as in the case of WT with the large spin density (30−40%) on the thiolate.[55] Therefore, we conclude that the low Cu A_{zz} value has a substantial contribution attributable to the nearly tetrahedral geometry[23] that increases the contribution of A_L, the orbital dipolar term to A_{zz} (see eq 1). This term depends on Δg_{zz} ($g_{zz} - g_e$), and Δg_{zz} is ∼30% larger in C112D/M121X (X = L, F) than in C112D. Detailed DFT calculations of the various contributions to Cu A_{zz} support the above interpretation (see ref 52). Nevertheless, the enhanced delocalization over the D112 carboxylate in type zero proteins relative to type 2 C112D adds weight to ET paths involving this residue. In pulse-radiolysis experiments monitoring ET from RSSR^{-} at C3/C26 to Cu^{II}, k_{et} for C112D azurin was found to be 123 s^{-1}, while for C112D/M121L, k_{et} = 61 s^{-1}.[25] Earlier experiments reported k_{et} for WT azurin to be 44 s^{-1}.[56] Reorganization energies (WT $\lesssim$ C112D/M121L $\ll$ C112D) support prediction of the opposite trend in k_{et}. However, in WT azurin ET, routes through C112 and through H46 are equally weighted; the resulting pathway interference slows ET.[19] In C112D azurin, the D112 route is severely attenuated, leading to more efficient ET through H46. Larger electron delocalization over D112 in the type zero proteins suggests that coupling has been restored along the D112 route, thus slowing ET due to pathway interference.

CONCLUSIONS

Spin delocalization over the ligands of type zero Cu^{II} in the azurin double mutant C112D/M121 (X = L, F), as manifested by ligand hyperfine couplings, was compared with that of the corresponding single mutant C112D in which the Cu^{II} exhibits spectroscopic properties of a type 2 site. Using a variety of pulse EPR techniques, applied at W- and X-band frequencies on natural abundance samples and $^{13}C/^{15}N$ enriched samples, we determined the hyperfine couplings of directly coordinated histidine nitrogen nuclei and the corresponding remote nitrogen nuclei. The hyperfine couplings of the coordinated nitrogens in type zero Cu^{II} were found to be close to those of WT azurin and smaller than in C112D. In contrast, a significant ^{13}C hyperfine coupling of 9 MHz, assigned to the coordinated C112D carboxylate, was found to be larger (by ∼50%) than the largest ^{13}C hyperfine coupling observed in C112D, suggesting a larger spin density on the type zero coordinated C112D oxygen. No protons with exceptionally large ^{1}H hyperfine couplings were detected. From this comparison, we conclude that the spin delocalization of type zero copper over its ligands is not dramatically larger than in type 2 C112D, in contrast to WT azurin. This finding suggests that the relatively small A_{zz}(Cu) observed for type zero copper is largely attributable to the nearly tetrahedral geometry of type zero sites, manifested in an increased contribution of the orbital dipolar term to the hyperfine interaction, in contrast to WT, where the small A_{zz} value is primarily due to spin delocalization to the thiolate ligand.

ASSOCIATED CONTENT

Supporting Information

W-band ED-NMR and Davies ENDOR of $^{13}C/^{15}N$ enriched C112D and C112D/M121L, W-band HYSCORE spectra of C112D/M121X (X = L, F), W-band Davies ENDOR of $^{13}C/^{15}N$ enriched C112D measured at 3222 mT, ^{2}H Mims ENDOR spectra of C112D and C112D/M121L in D_2O solutions, a table with the assignment and frequencies observed (MHz) in the X-band HYSCORE spectra of the three mutants studied, and a table with the Cu−H distances obtained from the crystal structures and the corresponding ^{1}H dipolar coupling. This material is available free of charge via the Internet at http://pubs.acs.org.

AUTHOR INFORMATION

Corresponding Author

*Email: Daniella.goldfarb@weizmann.ac.il.

Present Addresses

§Department of Chemistry and Chemical Biology, Cornell University, Ithaca, New York 4853.

⊥Laboratory of Chemical Physics, National Institute of Diabetes and Digestive and Kidney Diseases, National Institute of Health, Bethesda, Maryland 20892-0520.

Notes

The authors declare no competing financial interest.

ACKNOWLEDGMENTS

This work was supported by U.S.−Israel Binational Science Foundation (2006179) (D.G.) and was made possible in part by the historic generosity of the Harold Perlman Family (D.G.). D.G. holds the Erich Klieger Professorial Chair in Chemical Physics. Work at Caltech was supported by NIH DK019038.

REFERENCES

(1) Banci, L.; Bertini, I.; Luchinat, C.; Turano, P. In *Biological Inorganic Chemistry: Structure and Reactivity*; Bertini, I, Gray, H. B.,

Stiefel, E. I., Valentine, J. S., Eds.; University Press: Sausalito, CA, 2007; pp 229−277.
(2) Dennison, C. *Coord. Chem. Rev.* **2005**, *249*, 3025−3054.
(3) Gray, H. B.; Malmstrom, B. G.; Williams, R. J. P. *J. Biol. Inorg. Chem.* **2000**, *5*, 551−559.
(4) Quintanar, L.; Stoj, C.; Taylor, A. B.; Hart, P. J.; Kosman, D. J.; Solomon, E. I. *Acc. Chem. Res.* **2007**, *40*, 445−452.
(5) Solomon, E. I.; Sundaram, U. M.; Machonkin, T. E. *Chem. Rev.* **1996**, *96*, 2563−2605.
(6) Andrew, C. R.; SandersLoehr, J. *Acc. Chem. Res.* **1996**, *29*, 365−372.
(7) Colman, P. M.; Freeman, H. C.; Guss, J. M.; Murata, M.; Norris, V. A.; Ramshaw, J. A. M.; Venkatappa, M. P. *Nature* **1978**, *272*, 319−324.
(8) Farver, O.; Pecht, I. *Coord. Chem. Rev.* **2011**, *255*, 757−773.
(9) Gray, H. B.; Winkler, J. R. *Biochim. Biophys. Acta* **2010**, *1797*, 1563−1572.
(10) Holwerda, R. A.; Wherland, S.; Gray, H. B. *Annu. Rev. Biophys. Bioeng.* **1976**, *5*, 363−396.
(11) Nar, H.; Messerschmidt, A.; Huber, R.; Vandekamp, M.; Canters, G. W. *J. Mol. Biol.* **1991**, *221*, 765−772.
(12) Solomon, E. I. *Inorg. Chem.* **2006**, *45*, 8012−8025.
(13) Coremans, J. W. A.; Poluektov, O. G.; Groenen, E. J. J.; Canters, G. W.; Nar, H.; Messerschmidt, A. *J. Am. Chem. Soc.* **1996**, *118*, 12141−12153.
(14) Malmström, B. G. *Eur. J. Biochem.* **1994**, *223*, 711−718.
(15) Yanagisawa, S.; Banfield, M. J.; Dennison, C. *Biochemistry* **2006**, *45*, 8812−8822.
(16) Solomon, E. I.; Hare, J. W.; Dooley, D. M.; Dawson, J. H.; Stephens, P. J.; Gray, H. B. *J. Am. Chem. Soc.* **1980**, *102*, 168−178.
(17) George, S. J.; Lowery, M. D.; Solomon, E. I.; Cramer, S. P. *J. Am. Chem. Soc.* **1993**, *115*, 2968−2969.
(18) Shadle, S. E.; Pennerhahn, J. E.; Schugar, H. J.; Hedman, B.; Hodgson, K. O.; Solomon, E. I. *J. Am. Chem. Soc.* **1993**, *115*, 767−776.
(19) Regan, J. J.; Dibilio, A. J.; Langen, R.; Skov, L. K.; Winkler, J. R.; Gray, H. B.; Onuchic, J. N. *Chem. Biol.* **1995**, *2*, 489−496.
(20) Gewirth, A. A.; Cohen, S. L.; Schugar, H. J.; Solomon, E. I. *Inorg. Chem.* **1987**, *26*, 1133−1146.
(21) Abragam, A.; Pryce, M. H. L. *Proc. R. Soc. London, Ser. A* **1951**, *205* (12), 135.
(22) DiBilio, A. J.; Hill, M. G.; Bonander, N.; Karlsson, B. G.; Villahermosa, R. M.; Malmström, B. G.; Winkler, J. R.; Gray, H. B. *J. Am. Chem. Soc.* **1997**, *119*, 9921−9922.
(23) Lancaster, K. M.; Yokoyama, K.; Richards, J. H.; Winkler, J. R.; Gray, H. B. *Inorg. Chem.* **2009**, *48*, 1278−1280.
(24) Lancaster, K. M.; George, S. D.; Yokoyama, K.; Richards, J. H.; Gray, H. B. *Nature Chem.* **2009**, *1*, 711−715.
(25) Lancaster, K. M.; Farver, O.; Wherland, S.; Crane, E. J. III; Richards, J. H.; Pecht, I.; Gray, H. B. *J. Am. Chem. Soc.* **2011**, *133*, 4865−4873.
(26) Goldfarb, D.; Lipkin, Y.; Potapov, A.; Gorodetsky, Y.; Epel, B.; Raitsimring, A. M.; Radoul, M.; Kaminker, I. *J. Magn. Reson.* **2008**, *194* (1), 8−15.
(27) Davies, E. R. *Phys. Lett. A* **1974**, *A 47*, 1−2.
(28) Mims, W. B. *Proc. R. Soc. London, Ser. A* **1965**, *283*, 452−.
(29) Epel, B.; Arieli, D.; Baute, D.; Goldfarb, D. *J. Magn. Reson.* **2003**, *164*, 78−83.
(30) Epel, B.; Gromov, I.; Stoll, S.; Schweiger, A.; Goldfarb, D. *Conc. Magn. Reson. Part B* **2005**, *26B*, 36−45.
(31) Schosseler, P.; Wacker, T.; Schweiger, A. *Chem. Phys. Lett.* **1994**, *224*, 319−324.
(32) Höfer, P.; Grupp, A.; Nebenfuhr, H.; Mehring, M. *Chem. Phys. Lett.* **1986**, *132*, 279−282.
(33) Gemperle, C.; Aebli, G.; Schweiger, A.; Ernst, R. R. *J. Magn. Reson.* **1990**, *88*, 241−256.
(34) Radoul, M.; Sundararajan, M.; Potapov, A.; Riplinger, C.; Neese, F.; Goldfarb, D. *Phys. Chem. Chem. Phys.* **2010**, *12*, 7276−7289.
(35) Goldfarb, D.; Kevan, L. *J. Magn. Reson.* **1988**, *76*, 276−286.
(36) Flanagan, H. L.; Singel, D. J. *J. Chem. Phys.* **1987**, *87*, 5606−5616.
(37) Kofman, V.; Farver, O.; Pecht, I.; Goldfarb, D. *J. Am. Chem. Soc.* **1996**, *118*, 1201−1206.
(38) Grimaldi, S.; Ostermann, T.; Weiden, N.; Mogi, T.; Miyoshi, H.; Ludwig, B.; Michel, H.; Prisner, T. F.; MacMillan, F. *Biochemistry* **2003**, *42*, 5632−5639.
(39) van Gastel, M.; Coremans, J. W. A.; Jeuken, L. J. C.; Canters, G. W.; Groenen, E. J. J. *J. Phys. Chem. A* **1998**, *102*, 4462−4470.
(40) Kita, S.; Uchida, K.; Miyamoto, R.; Iwaizumi, M. *Chem. Lett.* **1992**, 1329−1332.
(41) Coremans, J. W. A.; Poluektov, O. G.; Groenen, E. J. J.; Canters, G. W.; Nar, H.; Messerschmidt, A. *J. Am. Chem. Soc.* **1997**, *119*, 4726−4731.
(42) Coremans, J. W. A.; Poluektov, O. G.; Groenen, E. J. J.; Canters, G. W.; Nar, H.; Messerschmidt, A. *J. Am. Chem. Soc.* **1996**, *118*, 12141−12153.
(43) Potapov, A.; Epel, B.; Goldfarb, D. *J. Chem. Phys.* **2008**, 128.
(44) Florent, M.; Kaminker, I.; Nagarajan, V.; Goldfarb, D. *J. Magn. Reson.* **2011**, *210*, 192−199.
(45) Kaminker, I.; Goldberg, H.; Neumann, R.; Goldfarb, D. *Chem.—Eur. J. 16*, 10014−10020.
(46) Fittipaldi, M.; Garcia-Rubio, I.; Trandafir, F.; Gromov, I.; Schweiger, A.; Bouwen, A.; Van Doorslaer, S. *J. Phys. Chem. B* **2008**, *112*, 3859−3870.
(47) Kulik, L.; Epel, B.; Messinger, J.; Lubitz, W. *Photosynth. Res.* **2005**, *84*, 347−353.
(48) Mino, H.; Ono, T. *Appl. Magn. Reson.* **2003**, *23*, 571−583.
(49) Potapov, A.; Pecht, I.; Goldfarb, D. *Chem. Chem. Phys.* **2010**, *12*, 62−65.
(50) Gromov, I.; Marchesini, A.; Farver, O.; Pecht, I.; Goldfarb, D. *Eur. J. Biochem.* **1999**, *266*, 820−830.
(51) Werst, M. M.; Davoust, C. E.; Hoffman, B. M. *J. Am. Chem. Soc.* **1991**, *113*, 1533−1538.
(52) Lancaster K. M.; Zaballa M. E.; Sproules S.; Sundararajan, M.; DeBeer, S.; Vila A. J.; Richards, J. H.; Neese, F.; Gray H. B. Submitted
(53) Schosseler, P. M.; Wehrli, B.; Schweiger, A. *Inorg. Chem.* **1997**, *36*, 4490−4499.
(54) Jeevarajan, A. S.; Carmichael, I.; Fessenden, R. W. *J. Phys. Chem.* **1990**, *94*, 1372−1376.
(55) Bottcher, R.; Kirmse, R.; Stach, J.; Keijzers, C. P. *Mol. Phys.* **1985**, *55*, 1431−1445.
(56) Fittipaldi, M.; Warmerdam, G. C. M.; de Waal, E. C.; Canters, G. W.; Cavazzini, D.; Rossi, G. L.; Huber, M.; Groenen, E. J. J. *Chemphyschem* **2006**, *7*, 1286−1293.
(57) Farver, O.; Pecht, I. *Proc. Natl. Acad. Sci. U.S.A.* **1989**, *86*, 6968−6972.
(58) Baute, D.; Arieli, D.; Neese, F.; Zimmermann, H.; Weckhuysen, B. M.; Goldfarb, D. *J. Am. Chem. Soc.* **2004**, *126*, 11733−11745.
(59) Kirmse, R.; Abram, U.; Bötther, R. *Chem. Phys. Lett.* **1982**, *88*, 98−102.
(60) Kirmse, R.; Abram, U.; Böttcher, R. *Chem. Phys. Lett.* **1982**, *90*, 9−12.